

ACOPERIREA NANOPARTICULELOR DE MAGNETITĂ CU STRAT DE SILICE MEZOPOROASĂ CU PORI DE DIMENSIUNI ȘI GEOMETRII DIFERITE COATING MAGNETITE NANOPARTICLES WITH MESOSTRUCTURED SILICA SHELL OF DIFFERENT PORE SIZE AND GEOMETRY

RAUL-AUGUSTIN MITRAN^{1,2}, DOINA GEORGESCU², NICOLAE STĂNICĂ¹,
CRISTIAN MATEI², DANIELA BERGER^{2*}

¹Romanian Academy, "Ilie Murgulescu" Institute of Physical Chemistry, Splaiul Independentei 202, Bucharest, 060021, Romania
²University "Politehnica" of Bucharest, Department of Inorganic Chemistry, Physical Chemistry & Electrochemistry, 1-7 Polizu street, Bucharest, 011061, Romania

Composite nanomaterials combining magnetic properties and porosity have various applications as catalysts, in targeted drug delivery, depollution, energy storage etc. However, the synthesis of magnetite nanoparticles coated with SBA-16-type mesoporous silica is very challenging due to the acidic medium required, which leads to the dissolution of iron oxides. Here, we report a simple synthesis of Fe_3O_4 @SBA-16 composite with high content of magnetic nanoparticles in a weak acidic medium. The influence of reagents addition order was also studied. The resulting materials have been investigated by small- and wide-angle X-ray diffraction, infrared spectroscopy, scanning electron microscopy, energy dispersive X-ray spectroscopy, nitrogen sorption analysis and magnetic measurements. The properties of Fe_3O_4 @SBA-16 samples are discussed and compared with a Fe_3O_4 @MCM-41 material, obtained in basic medium. All magnetic composites present high porosity and superparamagnetic behavior.

Nanomaterialele compozite care combină proprietățile magnetice cu porozitatea au diverse aplicații în cataliză, eliberare țintită de medicamente, depoluare, stocare de energie etc. Totuși, sinteza nanoparticulelor de magnetită acoperite cu silice mezoporoasă de tip SBA-16 este foarte dificilă din cauza mediului puternic acid, care conduce la dizolvarea oxidului de fier. În această lucrare raportăm o sinteză simplă pentru compozite Fe_3O_4 @SBA-16 cu conținut ridicat de magnetită într-un mediu slab acid. Influența ordinii adăugării reactivilor a fost studiată, iar materialele rezultate au fost caracterizate prin difracție de raze X la unghiuri mici și mari, spectroscopie în infraroșu, microscopie electronică de baleiaj, spectroscopie de raze X de energie dispersivă, izoterme de adsorbție-desorbție a azotului și măsurători magnetice. Proprietățile probelor Fe_3O_4 @SBA-16 sunt discutate comparativ cu un material Fe_3O_4 @MCM-41 obținut în mediu bazic. Toate nanocompozitele au porozitate ridicată și proprietăți superparamagnetice.

Keywords: superparamagnetic, mesoporous silica, SBA-16, Fe_3O_4 @SBA-16, magnetite, MCM-41

1. Introduction

Ever since their discovery in 1991 [1], ordered mesoporous materials have attracted significant interest because of their excellent properties, which include high surface areas and high pore volumes, narrow pore size distribution, biocompatibility and an easy way to tailor these properties through chemical synthesis [2,3]. Ordered mesoporous materials have been investigated for different applications including drug delivery [4-7], catalysis [8-10], depollution [11-14] or energy storage [15-17]. A valuable strategy to extend the useful properties of mesoporous silica materials (mSiO_2) is the synthesis of core-shell composites [18,19]. For example, magnetite coated with mesoporous silica preserves the good biocompatibility, textural and mechanical properties of the silica matrix, while Fe_3O_4 offers magnetic

properties. Fe_3O_4 - mSiO_2 composite materials open up applications such as targeted drug delivery [20], magnetic resonance imaging contrast agents [21], recoverable heterogeneous catalysts [22] or localized hyperthermia [23]. Fe_3O_4 nanoparticles exhibit superparamagnetic behavior, with single magnetic domains per nanoparticles and smaller saturation magnetization than bulk magnetite [24].

Regarding the mesoporous silica component of the Fe_3O_4 - mSiO_2 nanocomposites, most studies so far have focused on hexagonally ordered MCM-41 and SBA-15 materials with 2D pore networks [25,26]. Mesoporous materials with interconnected 3D pores (SBA-16, FDU-12, MCM-48 etc.) present some advantages over MCM-41 and SBA-15, related to better diffusion and transport properties [27]. So far, there is only one study detailing the preparation of Fe_3O_4 @SBA-16 materials.[28] This lack of literature reports stems

* Autor corespondent/Corresponding author,
E-mail: danaberger01@yahoo.com

from the narrow range of experimental conditions in which SBA-16 can be obtained, involving the use of strong acidic medium (~2M HCl) [29] and thus leading to the dissolution of the Fe₃O₄ nanoparticles.

In order to prepare magnetic mesoporous inorganic composites for medical applications, the synthesis of highly water dispersible superparamagnetic magnetite nanoparticles (NP) with a very narrow size distribution is very important. The colloidal synthesis method enables the synthesis of nanocrystals with controlled morphology. Here we report the preparation of mesostructured silica coated magnetite NP in a two step procedure for biomedical applications. Moreover, we present a method for obtaining Fe₃O₄@SBA-16 materials with good pore order, porosity and magnetic properties.

2. Experimental

2.1. Materials

Tetraethyl orthosilicate (TEOS, Fluka), poly(ethylene glycol)-block-poly(propylene glycol)-block-poly(ethylene glycol), EO₁₀₁PO₅₆EO₁₀₁ (Pluronic F127, Sigma Aldrich), ammonia solution 25% (Scharlau), concentrated hydrochloric acid (Sigma Aldrich), trimethylhexadecylammonium bromide (CTAB, AlfaAesar), iron (II) sulfate (Sigma Aldrich) and iron (III) chloride (Sigma Aldrich) were used as received.

2.2. Synthesis of magnetite nanoparticles (Fe₃O₄ NP)

Fe₃O₄ NP were obtained in the presence of CTAB through co-precipitation of Fe²⁺ and Fe³⁺ salts. To a solution prepared by dissolution of 2.73 g CTAB in 60 mL ultrapure water, 18 mL 0.5 M aqueous solution of FeCl₃ and 24 mL 0.25 M FeSO₄ were added under mechanical stirring and inert atmosphere, at 40 °C. After 1 h, 20 mL of 25% (wt.) aqueous ammonia solution were poured in the solution containing Fe²⁺ and Fe³⁺ ions under argon atmosphere. The reaction mixture was stirred for 1 h at 40 °C and the resulting nanoparticles were washed with water and ethanol and recovered by magnetic decantation.

2.3. Coating Fe₃O₄ NP with MCM-41 silica (Fe₃O₄@MCM-41)

0.046 g Fe₃O₄ NP (0.2 mmol) were dispersed by ultrasonic treatment into a solution containing 0.600 g CTAB (1.64 mmol) and 2.5 mL ammonia in 30 mL water. 2.5 mL TEOS (11.2 mmol) were added and the reaction mixture was mechanically stirred at 40 °C for 24 h. The reaction mixture was hydrothermally treated at 150 °C for 24 h, followed by the solid separation and surfactant removal through extraction in a 2% (wt) ammonium nitrate alcoholic solution. The sample was labeled Fe₃O₄@MCM-41.

2.4. Coating Fe₃O₄ NP with SBA-16 silica (Fe₃O₄@SBA-16)

0.094 g Fe₃O₄ NP (0.4 mmol) were dispersed into 9.5 mL water containing 0.206 mg Pluronic F127. Then, 0.890 mL TEOS (4 mmol) was added under mechanical stirring. Before or after the TEOS addition 0.158 mL concentrated HCl was also added and the resulting samples are denoted "Fe₃O₄@SBA-16b" and "Fe₃O₄@SBA-16a", respectively. The sol was kept at 40 °C for 24 h, followed by ageing at 105 °C for 24 hours. The surfactant was removed by calcination in air at 550 °C for 5h.

2.5. Materials characterization

Small- and wide-angle X-ray powder diffraction (XRD) were recorded on Bruker D8 Discover and Rigaku Miniflex II diffractometers, equipped with CuK α radiation. FTIR spectra were carried out on Bruker Tensor 27 spectrometer (KBr pellets technique). Nitrogen adsorption-desorption isotherms were recorded at 77K on a Quantachrome Autosorb iQ₂ gas physisorption analyzer. The total pore volume was determined as cumulative pore volume for the entire isotherm. The specific surface area was calculated by Brunauer–Emmett–Teller (BET) theory from multi-point regression in the 0.1-0.3 relative pressure range, while the pore size distribution curves were determined by using the most suitable method depending on the pore array of silica coating. The synthesized materials were investigated by scanning electron microscopy (SEM) on a Tescan Vega 3 LM microscope equipped with an energy-dispersive X-ray (EDX) spectrometer. The magnetic properties were measured at room temperature recording the magnetic susceptibility function of magnetic field on a LakeShore 7404 vibrating sample magnetometer.

3. Results and discussion

The wide-angle XRD pattern of Fe₃O₄ NP shows the formation of the cubic magnetite phase with inverse spinel structure (ICDD 76-1849) as the only crystalline phase (Fig. 1). The unit cell parameter for magnetite phase computed from all diffraction peaks was 0.836 nm. The crystallite size of 11 nm was calculated using Rigaku PDXL software based on Scherrer's equation from all Bragg reflections for magnetite. For the Fe₃O₄@MCM-41, Fe₃O₄@SBA-16a and Fe₃O₄@SBA-16b composites, an additional broad peak between 15-35° 2 θ , corresponding to amorphous silica phase formation can be noticed. The crystallite size of magnetite phase was not altered after the silica coating procedure or the composite calcination.

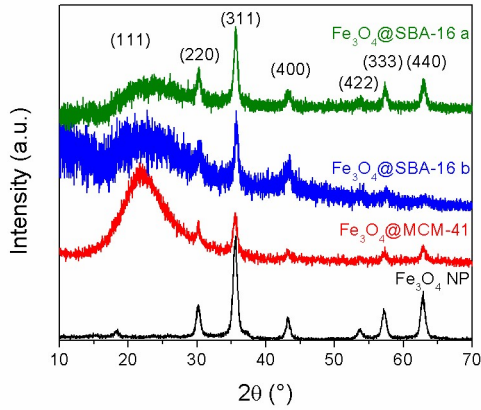


Fig. 1. - Wide-angle XRD patterns of Fe_3O_4 NP and silica-magnetite composites. / Difractogramele de raze X la unghiuri mari ale Fe_3O_4 NP și compozitelor silice-magnetită.

The small-angle diffraction pattern (Fig. 2A) of Fe_3O_4 @MCM-41 presents three characteristic peaks, indexed as the (100), (110) and (200) Bragg reflections of the hexagonal space group $P6m$. In the case of the Fe_3O_4 @SBA-16 composites, both

samples exhibits a well-defined (110) Bragg reflection, demonstrating an ordered mesopores array (Fig. 2B). In addition, the sample Fe_3O_4 @SBA-16a also presents a secondary diffraction peak, which could be indexed as the (200) Bragg reflection of the cubic $Im\bar{3}m$ space group (Fig. 2B, inset). The small-angle XRD results suggest that Fe_3O_4 @SBA-16a has a higher degree of mesopore order than Fe_3O_4 @SBA-16b.

The nitrogen adsorption-desorption isotherms (Fig. 3A) for Fe_3O_4 @MCM-41 and Fe_3O_4 @SBA-16a are type IV, characteristic for mesoporous materials [30]. The Fe_3O_4 @SBA-16a sample presents a H2-type hysteresis loop, typical for materials with ink-bottle mesopores. For Fe_3O_4 @MCM-41, a H1-type hysteresis, characteristic for independent pores with hexagonal arrangement, was observed. The pore size distribution curve is often calculated from the desorption branch of the isotherm by BJH theory, widely used to assess the pore size for mesoporous materials [31]. This approach is suitable for non-intersecting mesopores (as the case of MCM-41 materials), but generates false results for

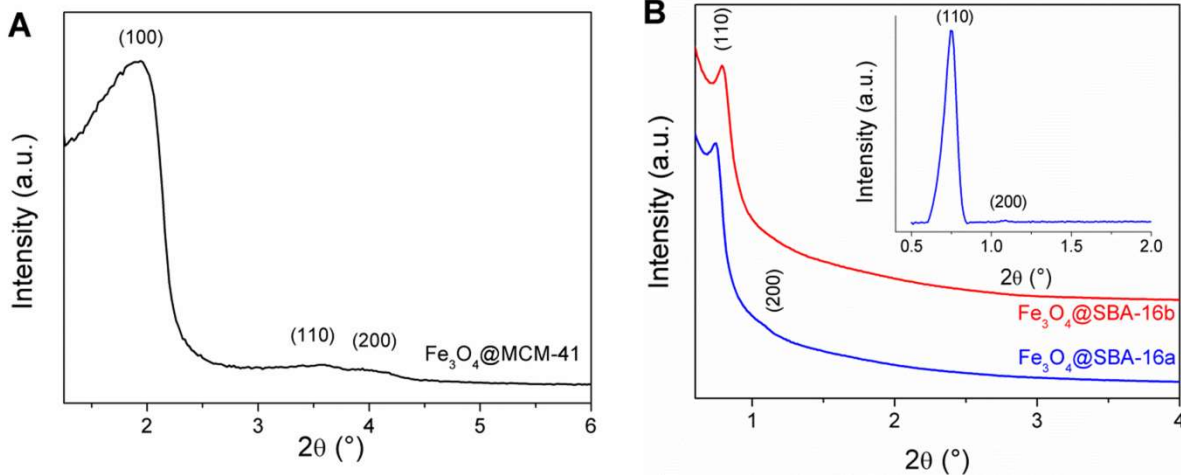


Fig. 2 - Small-angle XRD patterns of Fe_3O_4 @MCM-41 (A) and Fe_3O_4 @SBA-16-type composites (B). Inset, the pattern of Fe_3O_4 @SBA-16a with background subtracted (B). / Difractogramele de raze X la unghiuri mici ale compozitelor Fe_3O_4 @MCM-41 (A) și Fe_3O_4 @SBA-16 (B). Inserată, difractograma de raze X la unghiuri mici a probei Fe_3O_4 @SBA-16a cu linia de bază extrasă.

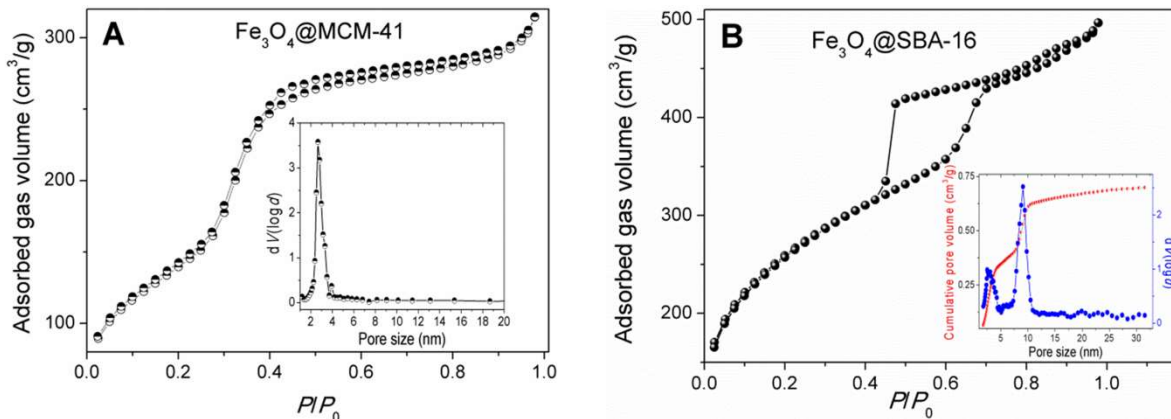


Fig. 3- N_2 adsorption-desorption isotherm and the corresponding pore size distribution curve for Fe_3O_4 @MCM-41 (A) and Fe_3O_4 @SBA-16a (B). / Izotermele de adsorbție-desorbție ale N_2 și distribuția de dimensiuni a porilor pentru Fe_3O_4 @MCM-41 (A) și Fe_3O_4 @SBA-16a (B).

Table 1

Unit cell parameter, specific surface area, total pore volume and average pore diameter values for the Fe₃O₄ nanoparticles and magnetite-silica materials / Parametrul celulei elementare, suprafața specifică, volumul total de pori și diametrul mediu al porilor pentru nanoparticulele de Fe₃O₄ și materialele magnetită-silice

Sample	a_0 (nm)*	S_{BET} (m ² /g)	V_{pore} (cm ³ /g)	d_{pore} (nm)
Fe ₃ O ₄ NP	0.836	67.4	-	-
Fe ₃ O ₄ @MCM-41	5.10	515	0.46	2.67
Fe ₃ O ₄ @SBA-16b	15.6	-	-	-
Fe ₃ O ₄ @SBA-16a	16.7	938	0.70	9.10

* $a_0=2d_{100}/\sqrt{3}$ for silica with hexagonal pore framework; $a_0=\sqrt{2}d_{110}$ for silica with cubic pore array

connected pores due to the tensile strength effect [32]. Therefore, for Fe₃O₄@SBA-16a composite, the pore size distribution curve was determined by non-local density functional theory (NLDFT) considering cylindrical/spherical pores, which is the most suitable method for the determination of pore dimension for ink-bottle mesopores [33,34].

The Fe₃O₄@SBA-16a sample exhibits a bimodal pore size distribution curve with the main peak centered at 9.1 nm and the total cumulative pore volume being 0.70 cm³/g (Fig. 3B).

The unit cell parameter values, a_0 , for magnetite NP and silica coating of the composite samples, as well as the textural parameters (specific surface area, S_{BET} , total pore volume, V_{pore} and average pore diameter, d_{pore}) were gathered in Table 1. The specific surface area and total pore volume are higher for Fe₃O₄@SBA-16a in comparison with Fe₃O₄@MCM-41 (Table 1), indicating higher porosity for the SBA-16a material.

The morphology of the synthesized materials was investigated through SEM analyses (Fig. 4 A, C, D). The Fe₃O₄ NP consists of

spherical particles with nanometric dimensions, which tend to form spherical agglomerates with a diameter in the range of 50-80 nm (Fig. 4 A). Larger spherical particles are observed in the case of all magnetite-silica composites (Fig. 4 B, C, D). In general, the composite particles are polydisperse in size, but their diameter is between 200 nm and 500 nm. A very good dispersion of the magnetite nanoparticles (bright spots) into the MCM-41 framework can be noticed for Fe₃O₄@MCM-41 (Fig. 4 B) in the back scatter electrons (BSE) detection mode. The EDX map of Fe₃O₄@SBA-16a (Fig. 4 E) also shows a good dispersion of Fe₃O₄ nanoparticles in the silica matrix. The ratio Fe:Si was found using EDX quantitative analyses in at least five different areas of each sample (Table 2) and it is lower than the initial ratio used in the synthesis. The yield in Fe₃O₄ was computed as 62% for Fe₃O₄@MCM-41 and 50% for Fe₃O₄@SBA-16a, with the lower value for the SBA-16 sample explained by the partial dissolution of the magnetite nanoparticles in the acidic synthesis medium.

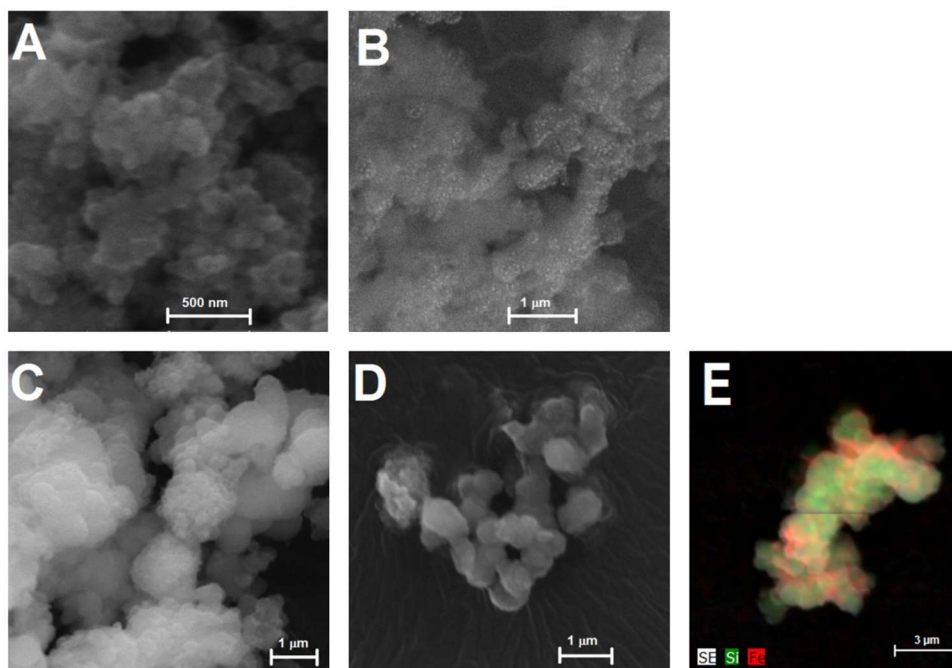


Fig. 4- SEM images of Fe₃O₄ NP (A), Fe₃O₄@MCM-41(B), Fe₃O₄@SBA-16b (C), Fe₃O₄@SBA-16a (D) și Fe₃O₄@SBA-16a cu distribuția elementelor.

FT-IR spectroscopy was used to assess the various chemical bonds present in the obtained materials (Fig. 5). The characteristic stretching vibrations associated with Fe-O bonds for the Fe₃O₄ NP are observed at 450, 580 and 630 cm⁻¹ and correspond to the Fe(II) and Fe(III) ions in both octahedral and tetrahedral geometries [35]. These bands can be also noticed in the silica-magnetite materials, proving the successful incorporation of magnetite in composites, even though the 450 cm⁻¹ Fe-O in octahedral geometry is superimposed with the 465 cm⁻¹ Si-O bending vibration. The presence of silica in the composite materials is indicated by its characteristic vibrations: Si-O-Si asymmetric stretching at ~1090 cm⁻¹, Si-O-Si symmetric stretching at ~800 cm⁻¹ and Si-OH deformation vibrations at ~960 cm⁻¹. All samples contain physisorbed water and surface hydroxyl groups, as evidenced by the 1640 cm⁻¹ water bending vibration and the broad 3450 cm⁻¹ O-H stretching vibration, respectively. Lastly, the existence of surfactant molecules for Fe₃O₄ NP and Fe₃O₄@SBA-16b can be inferred through the C-H stretching bands between 2850-2925 cm⁻¹ and the C-C and C-N vibrations in the 1200-1500 cm⁻¹ range.

The magnetic susceptibility measurements at room temperature of both magnetite nanoparticles and magnetite-mesoporous silica materials show typical superparamagnetic behavior, with anhysteretic behavior (Fig. 6). The magnetization (M) versus applied field (H) curves present a sharp increase in magnetization between -3000 and 3000 G for all samples, reaching saturation at around 4000 G. This behavior is characteristic for magnetite [25] and demonstrates the preservation of Fe₃O₄ phase in the nanocomposite samples. A high saturation magnetization is desired for the magnetite-silica composites for targeted drug delivery or catalysis. As expected, the saturation magnetization of Fe₃O₄ nanoparticles (59.8 emu/g) is lower than that of bulk magnetite (~95 emu/g) [24] due to the nanometer size of Fe₃O₄ NP.

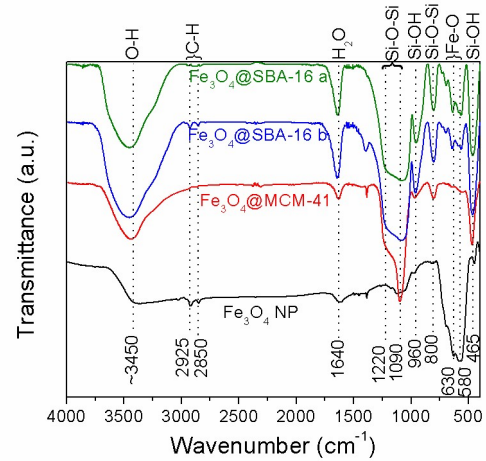


Fig. 5 - FT-IR spectra of magnetite nanoparticles and magnetite-silica composites/ Spectrele FT-IR ale nanoparticulelor de magnetită și a compozitelor magnetită-silice.

The saturation magnetization of Fe₃O₄@MCM-41 (5.2 emu/g) is lower than of Fe₃O₄@SBA-16a (9.9 emu/g), confirming the lower magnetite fraction in the former sample (Table 2). Keeping in mind that no changes in average crystallite size and phase composition were detected by XRD after the silica coating procedure of magnetic nanoparticles, the weight content of magnetite in the composite samples can be computed assuming that the saturation magnetization of these samples is given only by the magnetite phase (Table 2). A good correlation between EDX analyses and the saturation magnetization values were obtained for both samples, especially for the Fe₃O₄@SBA-16a composite. For Fe₃O₄@MCM-41, the content of magnetite phase computed from EDX analysis was 7.2% (wt), while from the saturation magnetization value it was 8.7% (wt). This difference can be explained by the fact that EDX analysis is a surface sensitive technique. Thus, only the Fe₃O₄ nanoparticles close to the particle surface are quantified by EDX. In the case of Fe₃O₄@SBA-16a sample, a content of Fe₃O₄ nanoparticles of 16% (wt.) was determined from

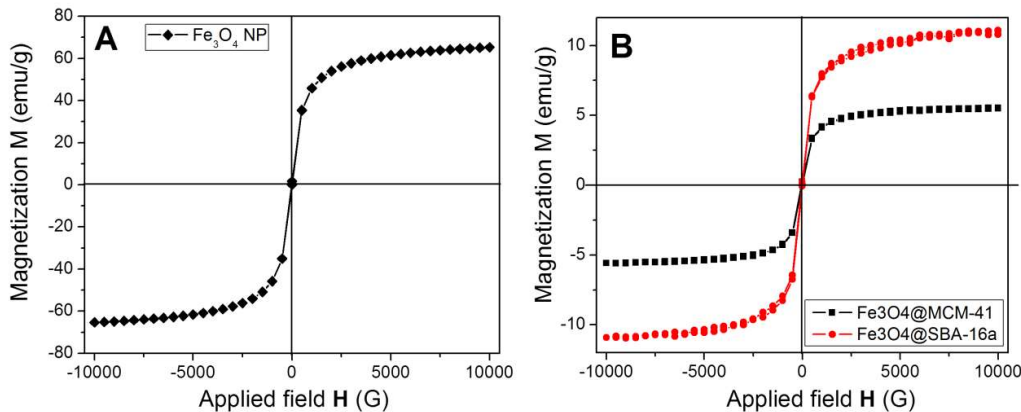


Fig. 6 - Magnetization versus applied field curves for A) Fe₃O₄ NP and B) magnetite-silica samples at 25°C/ Variația magnetizării în funcție de câmpul magnetic pentru A) Fe₃O₄ NP și B) probele magnetită-silice la 25°C.

Table 2

The saturation magnetization (M_s), mass susceptibility (χ_g) and Fe_3O_4 content computed from magnetic measurements or EDX analysis
Magnetizarea de saturație (M_s), susceptibilitatea masică (χ_g) și conținutul de Fe_3O_4 calculat din măsurători magnetice sau analiza EDX.

Sample	M_s (emu/g)	$\chi_g \cdot 10^6$ (cm^3/g)	Fe_3O_4 content from M_s (% wt.)	Fe_3O_4 content from EDX (% wt.)
Fe_3O_4 NP	59.81	14.00	-	-
Fe_3O_4 @MCM-41	5.24	1.52	8.7	7.2
Fe_3O_4 @SBA-16a	9.91	31.36	16.6	16

EDX analysis, while taking into account the saturation magnetization value the weight fraction of magnetic nanoparticles is 16.6% (wt.). The very close magnetite content values of the Fe_3O_4 @SBA-16a composite could be explained by a thin silica coating of Fe_3O_4 nanoparticles.

The magnetic susceptibility values of the investigated samples present the same variation as the saturation magnetization, decreasing in the order Fe_3O_4 NP > Fe_3O_4 @SBA-16a > Fe_3O_4 @MCM-41 (Table 2).

4. Conclusions

Mesostructured magnetite-silica composites with cubic, interconnected (SBA-16) or hexagonal, disconnected (MCM-41) pore systems have been obtained and characterized. The pore order and magnetite crystallinity in the case of cubic SBA-16 composites strongly depends on the synthesis method. Higher pore order was obtained by adding HCl after the silica precursor, decreasing the magnetite dissolution in the reaction media through competition with TEOS hydrolysis. The magnetite-cubic ordered silica sample retains ~50% of the initial magnetite nanoparticles, as evidenced by EDX and magnetic susceptibility measurements and exhibits a good saturation magnetization (~10 emu/g), specific surface area (938 m^2/g) and total pore volume (0.70 cm^3/g). The magnetic properties, structural and textural properties of the Fe_3O_4 @SBA-16 material obtained in acid media compares favorably with Fe_3O_4 @MCM-41 synthesized in basic conditions, where iron dissolution from the magnetite nanoparticles is suppressed. Thus, the Fe_3O_4 @SBA-16 material obtained using the presented method is a promising candidate for applications requiring large porosity and saturation magnetization, such as targeted drug delivery, heterogeneous catalysis or depollution.

Acknowledgements

The financial support of the Romanian project PCCA no. 131/2012 is greatly appreciated.

REFERENCES

- C. T. Kresge; M. E. Leonowicz; W. J. Roth; J. C. Vartuli; J. S. Beck, Ordered mesoporous molecular sieves synthesized by a liquid-crystal template mechanism, *Nature*, 1992, **359** (6397), 710.
- N. Ehlert; P. P. Mueller; M. Stieve; T. Lenarz; P. Behrens, Mesoporous silica films as a novel biomaterial: applications in the middle ear, *Chemical Society Reviews*, 2013, **42** (9), 3847.
- M. Choi; W. Heo; F. Kleitz; R. Ryoo, Facile synthesis of high quality mesoporous SBA-15 with enhanced control of the porous network connectivity and wall thickness, *Chemical Communications*, 2003, (12), 1340.
- M. Vallet-Regí; A. Rámila; R. P. del Real; J. Pérez-Pariente, A new property of MCM-41: Drug delivery system, *Chemistry of Materials*, 2001, **13** (2), 308.
- F. Tang; L. Li; D. Chen, Mesoporous silica nanoparticles: synthesis, biocompatibility and drug delivery, *Advanced Materials*, 2012, **24** (12), 1504.
- M. Vallet-Regí; F. Balas; D. Arcos, Mesoporous materials for drug delivery, *Angewandte Chemie International Edition*, 2007, **46** (40), 7548.
- D. Berger; L. Bajenaru; S. Nastase; R.-A. Mitran; C. Munteanu; C. Matei, Influence of structural, textural and surface properties of mesostructured silica and aluminosilicate carriers on aminoglycoside uptake and in vitro delivery, *Microporous and Mesoporous Materials*, 2015, **206**, 150.
- C. M. A. Parlett; P. Keshwala; S. G. Wainwright; D. W. Bruce; N. S. Hondow; K. Wilson; A. F. Lee, Hierarchically ordered nanoporous Pd/SBA-15 catalyst for the aerobic selective oxidation of sterically challenging allylic alcohols, *ACS Catalysis*, 2013, **3** (9), 2122.
- C. Comănescu, Synthesis and characterization of novel mesocomposites Co_3O_4 and CuO @OMS (ordered mesoporous silica) as active catalysts for hydrocarbon oxidation, *Journal of Nanoparticle Research*, 2014, **16** (3), 1.
- A. Kumar; D. Nepak; D. Srinivas, Direct synthesis of amides from amines using mesoporous Mn-SBA-12 and Mn-SBA-16 catalysts, *Catalysis Communications*, 2013, **37** (0), 36.
- Y. Kim; J. Bae; J. Park; J. Suh; S. Lee; H. Park; H. Choi, Removal of 12 selected pharmaceuticals by granular mesoporous silica SBA-15 in aqueous phase, *Chemical Engineering Journal*, 2014, **256** 475.
- A. R. Cestari; E. F. S. Vieira; G. S. Vieira; L. P. da Costa; A. M. G. Tavares; W. Loh; C. Airoidi, The removal of reactive dyes from aqueous solutions using chemically modified mesoporous silica in the presence of anionic surfactant — The temperature dependence and a thermodynamic multivariate analysis, *Journal of Hazardous Materials*, 2009, **161** (1), 307.
- K. Y. Ho; G. McKay; K. L. Yeung, Selective adsorbents from ordered mesoporous silica, *Langmuir*, 2003, **19** (7), 3019.
- A. Walcarius; L. Mercier, Mesoporous organosilica adsorbents: nanoengineered materials for removal of organic and inorganic pollutants, *Journal of Materials Chemistry*, 2010, **20** (22), 4478.
- S. Zheng; F. Fang; G. Zhou; G. Chen; L. Ouyang; M. Zhu; D. Sun, Hydrogen storage properties of space-confined NaAlH_4 nanoparticles in ordered mesoporous silica, *Chemistry of Materials*, 2008, **20** (12), 3954.
- R. A. Mitran; D. Berger; C. Munteanu; C. Matei, Evaluation of different mesoporous silica supports for energy storage in shape-stabilized phase change materials with dual thermal responses, *The Journal of Physical Chemistry C*, 2015, **119** (27), 15177.

17. L. Zhang; H. Shi; W. Li; X. Han; X. Zhang, Structure and thermal performance of poly(ethylene glycol) alkyl ether (Brij)/porous silica (MCM-41) composites as shape-stabilized phase change materials, *Thermochimica Acta*, 2013, **570**, 1.
18. Y. Chen; H. Chen; D. Zeng; Y. Tian; F. Chen; J. Feng; J. Shi, Core/shell structured hollow mesoporous nanocapsules: a potential platform for simultaneous cell imaging and anticancer drug delivery, *ACS Nano*, 2010, **4** (10), 6001.
19. M. Petrescu; R. A. Mitran; A. M. Luchian; C. Matei; D. Berger, Mesoporous ceria-silica composites as carriers for doxycycline, *UPB Scientific Bulletin, Series B: Chemistry and Materials Science*, 2015, **77** (3), 13.
20. M. Arruebo; R. Fernández-Pacheco; M. R. Ibarra; J. Santamaría, Magnetic nanoparticles for drug delivery, *Nano Today*, 2007, **2** (3), 22.
21. J. Kim; H. S. Kim; N. Lee; T. Kim; H. Kim; T. Yu; I. C. Song; W. K. Moon; T. Hyeon, Multifunctional uniform nanoparticles composed of a magnetite nanocrystal core and a mesoporous silica shell for magnetic resonance and fluorescence imaging and for drug delivery, *Angewandte Chemie International Edition*, 2008, **47** (44), 8438.
22. W. Li; B. Zhang; X. Li; H. Zhang; Q. Zhang, Preparation and characterization of novel immobilized $\text{Fe}_3\text{O}_4@\text{SiO}_2@m\text{SiO}_2$ -Pd(0) catalyst with large pore-size mesoporous for Suzuki coupling reaction, *Applied Catalysis A: General*, 2013, **459**, 65.
23. K. C. Souza; N. D. S. Mohalle; E. M. B. Sousa, Mesoporous silica-magnetite nanocomposite: facile synthesis route for application in hyperthermia, *Journal of Sol-Gel Science and Technology*, 2009, **53** (2), 418.
24. W. Pei; H. Kumada; T. Natusme; H. Saito; S. Ishio, Study on magnetite nanoparticles synthesized by chemical method, *Journal of Magnetism and Magnetic Materials*, 2007, **310** (2, Part 3), 2375.
25. H. H. P. Yiu; M. A. Keane; Z. A. D. Lethbridge; M. R. Lees; A. J. E. Haj; J. Dobson, Synthesis of novel magnetic iron metal-silica (Fe-SBA-15) and magnetite-silica (Fe_3O_4 -SBA-15) nanocomposites with a high iron content using temperature-programmed reduction, *Nanotechnology*, 2008, **19** (25), 255606.
26. X. Zang; W. Xie, Enzymatic interesterification of soybean oil and methyl stearate blends using lipase immobilized on magnetic Fe_3O_4 /SBA-15 composites as a biocatalyst, *Journal of Oleo Science*, 2014, **63** (10), 1027.
27. A. Popat; J. Liu; Q. Hu; M. Kennedy; B. Peters; G. Q. Lu; S. Z. Qiao, Adsorption and release of biocides with mesoporous silica nanoparticles, *Nanoscale*, 2012, **4** (3), 970.
28. R. C. S. Azevedo; R. G. Sousa; W. A. A. Macedo; E. M. B. Sousa, Combining mesoporous silica-magnetite and thermally-sensitive polymers for applications in hyperthermia, *Journal of Sol-Gel Science and Technology*, 2014, **72** (2), 208.
29. D. Zhao; Q. Huo; J. Feng; B. F. Chmelka; G. D. Stucky, Nonionic triblock and star diblock copolymer and oligomeric surfactant syntheses of highly ordered, hydrothermally stable, mesoporous silica structures, *Journal of the American Chemical Society*, 1998, **120** (24), 6024.
30. K. S. W. Sing, Reporting physisorption data for gas/solid systems with special reference to the determination of surface area and porosity (Recommendations 1984). *Pure and Applied Chemistry*, 1985, **57**, 603.
31. J. C. Groen; L. A. A. Peffer; J. Pérez-Ramírez, Pore size determination in modified micro- and mesoporous materials. Pitfalls and limitations in gas adsorption data analysis, *Microporous and Mesoporous Materials*, 2003, **60** (1-3), 1.
32. A. H. Janssen; A. J. Koster; K. P. de Jong, On the shape of the mesopores in zeolite Y: a three-dimensional transmission electron microscopy study combined with texture analysis, *The Journal of Physical Chemistry B*, 2002, **106** (46), 11905.
33. D. Carta, S. Bullita, M. F. Casula, A. Casu, A. Falqui, A. Corrias, Cubic mesoporous silica (SBA-16) prepared using butanol as the co-surfactant: A general matrix for the preparation of FeCo-SiO₂ nanocomposites, *ChemPlusChem* 2013, **78**, 364.
34. P. I. Ravikovitch; A. V. Neimark, Density functional theory of adsorption in spherical cavities and pore size characterization of templated nanoporous silicas with cubic and three-dimensional hexagonal structures, *Langmuir*, 2002, **18** (5), 1550.
35. P. E. G. Casillas; C. A. M. Pérez; C. A. R. Gonzalez, Infrared spectroscopy of functionalized magnetic nanoparticles. INTECH Open Access Publisher, 2012.

ANIVERSĂRI



20 septembrie (1459) – Ziua orașului București

La această dată se împlinesc 557 de ani de la prima atestare documentară a existenței Orașului București, într-un hrisov emis de cancelaria voievodului Vlad Țepeș. În ordine cronologică, orașul București a devenit treptat, în secolele următoare, cea de a patra capitală a Țării Românești a Munteniei (dupa Câmpulung, Curtea de Argeș și Târgoviște) și prima capitală a României Mari după Războiul de Întregire Națională din 1916 – 1918
